IEEE Access
Multidisciplinary | Rapid Review | Open Access Journal

Received January 2, 2021, accepted January 20, 2021, date of publication January 25, 2021, date of current version February 3, 2021.

Digital Object Identifier 10.1109/ACCESS.2021.3054426

Optimal Number of Turns Design of the IPT Coils for Laptop Wireless Charging

EUN S. LEE[1], (Member, IEEE), BYEONG G. CHOI[2], (Member, IEEE), MYUNG Y. KIM[1], (Member, IEEE), AND SEUNG H. HAN[3], (Member, IEEE)

[1]Propulsion System Research Team, Korea Railroad Research Institute, Uiwang 16105, South Korea
[2]Smart Device Team, Samsung Research, Seoul 06765, South Korea
[3]FlexPower Company Ltd., Suwon 16522, South Korea

Corresponding author: Eun S. Lee (eunsoo86@krri.re.kr)

This work was supported by the Railroad Technology Development Program funded by Ministry of Land, Infrastructure and Transport (MOLIT) of Korean Government, under Grant 21RTRP-B146051-04.

ABSTRACT The coil design of the inductive power transfer (IPT) for a transmitter (Tx) and receiver (Rx) is crucial to determine the performance of the IPT. Considering core loss and copper loss of the Tx and Rx coils, which are major loss terms of the whole IPT system, determination of the winding turns for the Tx and Rx coils becomes a key factor for maximum power transfer design of the IPT coils. In this paper, an optimal turns design of IPT coils for laptop wireless charging applications with a maximum power transfer efficiency is proposed. Under a specific design requirement of IPT, optimal turns of the Tx and Rx coils $N_{1,op}$ and $N_{2,op}$ can be determined by the proposed IPT coil design procedure with a finite-element-method (FEM) based simulation analysis. From the results of the coil design by the proposed IPT coil design methodology, $N_{1,op}$ and $N_{2,op}$ for maximum power efficiency, and input DC voltage V_{dc} for the target load power can be found by the proposed coil design procedure. The 40W prototypes of the two symmetry and asymmetry IPT coils for laptop wireless charging were fabricated, and verified by simulation and experiments. To separately verify the core and copper loss of the IPT coils, a resistance model and Steinmetz equation-based methods were comparatively evaluated, and it was found that they matched well at a core temperature condition of below 40°C. The results showed that the total weight and the thickness of the Tx and Rx coils as well as the maximum power efficiencies of 95.1% and 96.8% for the symmetry and asymmetry cases were obtained by the proposed IPT coil design procedure, which becomes a practical solution for the laptop wireless charging coil design.

INDEX TERMS Wireless power transfer (WPT), inductive power transfer (IPT), coil design, optimal turns design, laptop wireless charging, maximum power transfer efficiency.

I. INTRODUCTION

Convenient power transfer methods have been required since the advent of electricity in the 19th century [1]–[33]. A wire-type power transfer method using power cables has thus far been commonly employed due to its simple use and cost effectiveness. However, power cables spoil the beauty where they are deployed and expose customers to the risk of electric shock. As an alternative solution, inductive power transfer (IPT) has been widely used for various applications [1]–[33]. By virtue of providing a wire-free environment with electric safety, the IPT system is expected to be a viable solution for a convenient power transfer method. For designing the IPT system, a transmitter (Tx) and receiver (Rx) coil design is important to determine the performance of the IPT. In most cases, the installation space for Tx and Rx coils is restricted. In this light, an optimal coil design is highly recommended under a given physical dimension of the IPT application for operating at the maximum power transfer efficiency.

Contrary to the conventional transformer design, the IPT coil has a large air gap between the Tx and Rx coils. Most previous studies on coil design concentrated on designing coil shapes or coil structures to enhance the performance of the IPT [1]–[33]. Multiple orthogonal coil structures have been developed for omnidirectional wireless power transfer [1]–[4]. For wireless electric vehicle charging, DD or DDQ pads have been widely used for lateral misalignment

The associate editor coordinating the review of this manuscript and approving it for publication was Yuh-Shyan Hwang.

tolerance and highly efficient static and dynamic charging characteristics [5]–[10]. For other IPT applications for static and dynamic charging of large power vehicles, various coil shapes are used [11]–[14]. Additional resonant coils also can be used to achieve power transfer capability [15]–[20]. Long slim dipole-coils have been adopted to transfer the load power over long distance [4], [21]–[24]. Coreless coil structures may be preferred to remove core loss for efficient operation [25]–[27]. In such previous works, however, the number of turns for Tx and Rx coils is arbitrarily determined without a reasonable design standard. In this case, it is difficult to consider such IPT systems to be optimally designed for the Tx and Rx coils.

In order to obtain the high efficiency and the high power density by changing k and Q, the Pareto optimization proposed in [6] can be utilized. However, this idea in [6] focused on changing quality factor and magnetic coupling coefficient; thus, there are plenty of variables that can be considered to design the IPT system. Considering the determination of the number of turns, the efficiency characteristics including quality factors, which are function of winding turns, have been derived for better power transfer efficiency [31]. This research focuses on increasing the quality factor and the optimal number of turns are not eventually considered for maximum power efficiency operation. A general design procedure to find electrical parameters by a theoretical analysis for maximum coil-to-coil efficiency has been proposed [32]. However, this research assumes that the size and shapes of the Tx and Rx coils are symmetrical, i.e., physical dimension and the number of turns. This restricts the universal design methodology of the Tx and Rx coil turns. A design methodology to find coil winding parameters, e.g., the number of turns, conductor diameter, interval between wires, and so on, has been proposed for maximum coupling coefficient [33]. Due to numerous parameters and an iterative process, it is quite complicated to adopt this design process as a practical IPT solution. In addition, only the coupling coefficient is considered and the power efficiency is not validated in this research [33]. Most importantly, such proposed coil design methodologies are based on the coreless type Tx and Rx coils [31]–[33]. In this case, a theoretical analysis can predict the magnetic characteristics. Because most IPT systems utilize a high-frequency ferrite core, these methodologies may have limitations in practical WPT applications having a ferrite core. Furthermore, adopting a ferrite core in Tx and Rx coils makes the IPT system difficult to analyze due to the unpredictable radiation of the magnetic field and the non-linear property of the ferrite core [22], [23]. In particular, the reluctance of the air-gap between the Tx and Rx coil in the magnetic circuit becomes dominant [21]–[24]; the reluctance of the air-gap hence cannot be analytically modeled for a magnetic circuit if a ferrite core is adopted in the Tx and Rx coils.

In order to find the optimum turns of the IPT coils with ferrite cores for maximum power transfer efficiency, additional time-consuming experimental processes by changing all the number of cases inevitably must be implemented. Some studies focused on only designing a circuit driving method or impedance matching methods for the maximum power transfer efficiency, without considering the number of turns [28]–[30]. Although an optimal ampere-turns design can be found by the magnetic circuit analysis, the optimum number of turns for Tx and Rx coils is not specified yet [23]. Therefore, the optimum number of turns for the Tx and Rx coils should be determined, considering the core loss and copper loss of the Tx and Rx coils, under the given parameters.

FIGURE 1. Typical examples of the laptops with WPT.

In this paper, a coil design methodology of an IPT system for the laptop wireless charging applications is newly proposed, as shown in Fig. 1. The proposed coil design methodology can be generally adopted to determine the number of turns for operating at maximum power transfer efficiency. Because it is almost impossible to analyze the magnetic field by a theoretical analysis, a finite-element-method (FEM) based simulation tool is adopted to obtain the coil inductance, magnetic coupling coefficient, and coil resistance, which includes the core loss and copper loss of the IPT coils. In this paper, a planar spiral coil, which is widely used for IPT coils, is adopted for the laptop wireless charging. Design examples of symmetric and asymmetric coil structures for the Tx and Rx coils were built for 10V load voltage and 40W load power delivery conditions. The validity of the proposed IPT is verified by simulations and experiments, showing the universality of the proposed IPT design procedure and providing a practical solution to design an IPT system.

II. OPTIMAL TURNS DESIGN OF THE IPT

In this section, the static circuit analysis and a FEM simulation-based parameter analysis are explained to determine the optimal turns of the Tx and Rx coils. The typical configuration of the IPT system is shown in Fig. 2. High-frequency voltage source v_1 is generated by a high-frequency inverter, and the load voltage v_L is obtained by a high-frequency rectifier, as shown in Fig. 2. For the compensation network, i.e., resonant tanks, in the primary and secondary sides, series, parallel, or LLC resonant networks

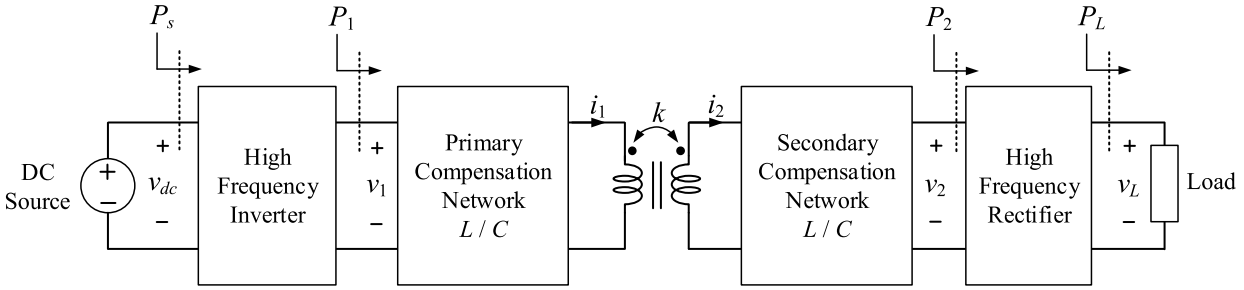

FIGURE 2. Schematic block diagram of the general IPT system.

can be used in accordance with the IPT and load characteristics [1]–[33]. As one of the typical design examples, a voltage source-based series-series resonant topology is adopted, as shown in Fig. 3, which is the most popular topology for various IPT applications [11]–[33]. Throughout this paper, it is assumed that high-frequency harmonics of voltages and currents in Fig. 3 are negligible and only fundamental components of voltage and currents are considered due to the primary and secondary compensation networks [5]–[33]. Throughout this paper, the high-frequency inverter and rectifier are assumed to be lossless and ideal to identify only the coil-to-coil efficiency. All the circuit parameters are assumed to be ideal unless otherwise specified.

A. EQUIVALENT CIRCUIT ANALYSIS OF THE IPT

The equivalent circuit of Fig. 3 can be expressed as in Fig. 4, where the primary and secondary turns are N_1 and N_2. Core loss and copper loss of the coils are reflected to the series resistance r_1 and r_2, where the equivalent modeling method is widely used to identify the core and copper losses in the coils [21]–[26], [31]. Self-inductance L_1 and L_2 in Fig. 3 is generally expressed by the magnetizing inductance L_m and leakage inductance L_{l1} and L_{l2} in Fig. 4, as follows:

$$L_1 = L_m + L_{l1}, \quad L_2 = n^2 L_m + L_{l2} \left(\because n \equiv \frac{N_2}{N_1} \right). \tag{1}$$

The rectifier with the load resistance in Fig. 3 is modeled as R_e, as shown in Fig. 4, considering only the fundamental frequency components of v_L and i_L under the continuous conduction mode (CCM) operation in the steady state [21]–[26], [38]–[42]. Thus, the voltage V_1, Rx coil current I_2, and equivalent load resistance R_e in Fig. 4 are expressed as follows:

$$V_1 = \alpha V_{dc}, \quad R_e = \alpha^2 R_L, \; I_2 = \frac{I_L}{\alpha}. \tag{2a}$$

$$\because \alpha = \frac{2\sqrt{2}}{\pi} \cong 0.9. \tag{2b}$$

Through applying the Thevenin's theorem to the left part of the circuit of Fig. 4, a simplified static circuit is obtained, as shown in Fig. 5(a). Assuming that $L_1\&C_1$ and $L_2\&C_2$ in Figs. 3-4 are fully resonated at the switching frequency for the maximum load power and load efficiency, $V_{m,th}$ and $R_{m,th}$ can be derived as follows:

$$V_{m,th} = \frac{jn^2\omega_s L_m}{r_1} V_1 \tag{3a}$$

$$R_{m,th} = \frac{(n\omega_s L_m)^2}{r_1} \tag{3b}$$

$$j\omega_s L_1 + \frac{1}{j\omega_s C_1} = 0, \quad j\omega_s L_2 + \frac{1}{j\omega_s C_2} = 0. \tag{3c}$$

From (3), a final equivalent circuit of the IPT from the load side viewpoint can be derived, as shown in Fig. 5(b). According to Fig. 5(b), the Rx current I_2 and the secondary power P_2 can be derived as follows:

$$I_2 = \frac{jn\omega_s L_m}{r_1(r_2 + R_e) + (n\omega_s L_m)^2} V_1 \tag{4a}$$

$$P_2 = I_2^2 R_e. \tag{4b}$$

On the other hand, to derive the primary power P_1 in Fig. 2, the proposed IPT circuit of Fig. 4 can be converted to Fig. 6(a) under the resonant condition of (3c), where $R_{L,th}$ can be derived as follows:

$$R_{L,th} = \frac{(n\omega_s L_m)^2}{r_2 + R_e}. \tag{5}$$

Assuming the fully resonance of L_1 and C_1 for maximum load power transfer in (3c), the final equivalent circuit of the IPT from the source side viewpoint can be derived, as shown in Fig. 6(b). The Tx current I_1 and the primary power P_1 can then be derived as follows:

$$I_1 = \frac{r_2 + R_e}{r_1(r_2 + R_e) + (n\omega_s L_m)^2} V_1 \tag{6a}$$

$$P_1 = V_1 I_1. \tag{6b}$$

From (4b) and (6b), a coil-to-coil efficiency η_c can be straightforwardly derived as follows:

$$\therefore \eta_c = \frac{P_2}{P_1} = \frac{(n\omega_s L_m)^2 R_e}{r_1(r_2 + R_e)^2 + (n\omega_s L_m)^2 (r_2 + R_e)}. \tag{7}$$

It is noteworthy that the coil-to-coil efficiency η_c, which excludes the loss of high-frequency inverter and the rectifier, is considered and verified for coil design verification throughout this paper. Only a voltage-source based series-series resonant topology is considered in this paper due to it having same principle as the other resonant topologies [21]–[26], [38].

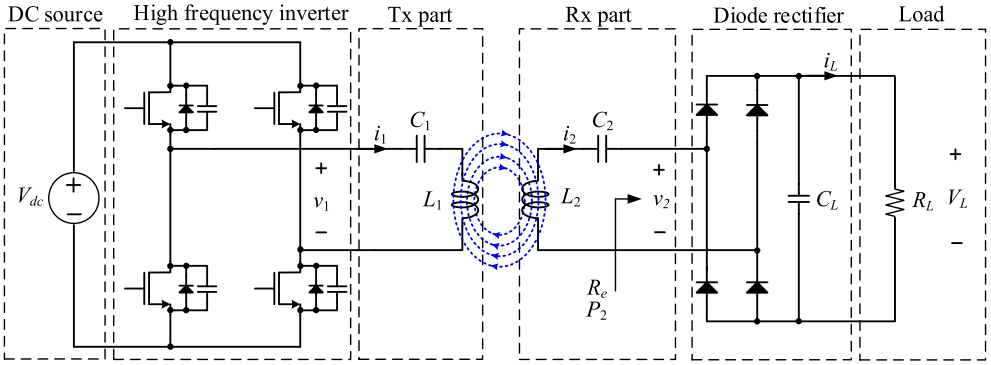

FIGURE 3. Circuit diagram of the voltage-source based series-series compensation topology of the IPT.

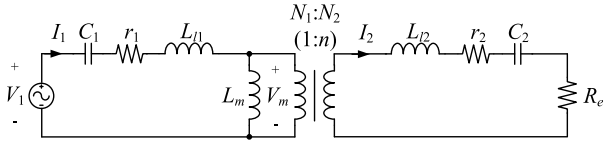

FIGURE 4. Equivalent circuit model of Fig. 3 based on the fundamental components of voltages and currents.

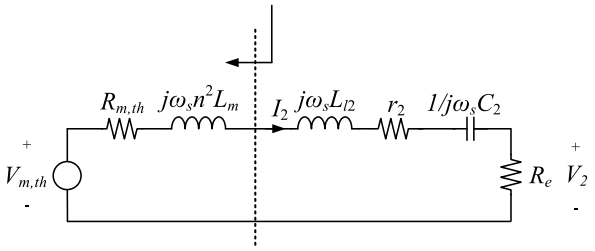

(a) Simplified circuit including the Thevenin equivalent circuit of $V_{m,th}$ and $R_{m,th}$ under the resonant condition of (3c).

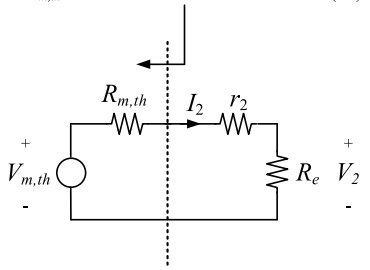

(b) Final equivalent circuit of the IPT, composed of pure resistance and a voltage source, under resonant condition of (3c).

FIGURE 5. Simplification of static circuits of Fig. 4 from the load side viewpoint.

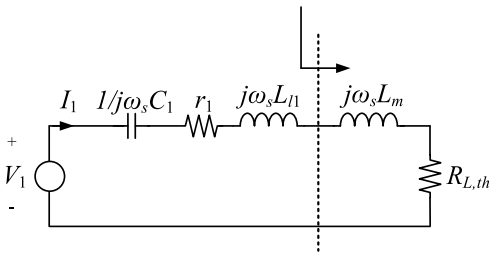

(a) Simplified circuit with $R_{L,th}$ under resonant condition of (3c)

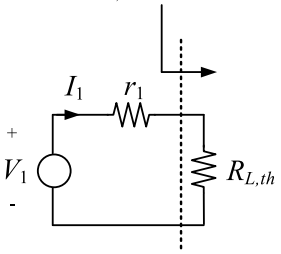

(b) Final equivalent circuit of the IPT under resonant condition of (3c)

FIGURE 6. Simplification of static circuits of Fig. 4 from the source side viewpoint.

TABLE 1. Design parameter goals for symmetry and asymmetry cases.

Electrical Parameters		Physical Parameters		
Parameters	Value	Parameters	Value	
			Symmetry	Asymmetry
V_L	10 V	l_{c1}	100 mm	100 mm
I_L	4.0 A	w_{c1}	100 mm	100 mm
R_L	2.5 Ω	l_{c2}	100 mm	95 mm
P_L	40 W	w_{c2}	100 mm	70 mm
f_s	100 kHz	d_c	40 mm	20 mm

B. FINITE-ELEMENT-METHOD SIMULATION BASED PARAMETER ANALYSIS

From (7), it is noted that the efficiency depends on r_1, r_2, N_1, N_2, and L_m under the given parameter goal, i.e., switching frequency f_s, load resistance R_L. It is almost impossible to exactly derive the parameters of r_1, r_2, and L_m by a theoretical analysis due to non-linear characteristics of the magnetic field distortion through the ferrite core and air [21]–[23]. In addition, it is too time-consuming to perform an experimental process by changing N_1 and N_2 with resonant conditions of (3c) in order to find the maximum efficiency point. Thus, a FEM based Maxwell simulation analysis has been performed throughout this paper.

To apply the proposed IPT design process for finding N_1 and N_2, it is assumed that the design parameters are given for the laptop wireless charging applications, as listed in Table 1.

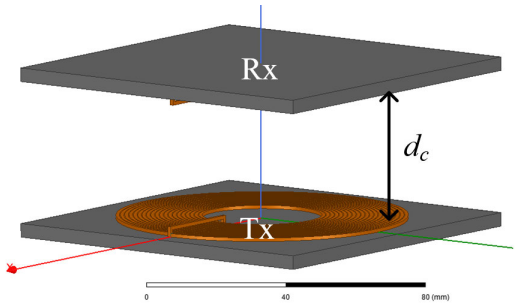

(a) Simulation model of Tx and Rx coils for the symmetrical case.

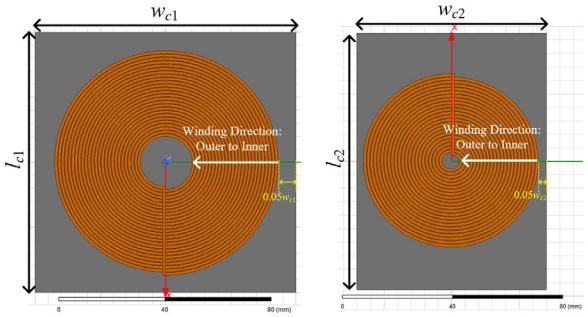

(b) The physical size of Tx coil (left) and Rx coil (right) for the asymmetrical case.

FIGURE 7. Simulation configuration of the IPT for varying the number of turns for Tx and Rx coils.

In general, electrical parameters are defined by load characteristics in laptop side, and physical parameters are determined by an allowable installation space in the laptop. It is noteworthy that the installation space for the Rx coil in laptop is quite tough, contrary to the Tx coil case; hence, symmetrical and asymmetrical structures for the different size of the Rx coils are comparatively evaluated in this paper to show the universality of the proposed coil design methodologies. The symmetrical structure means that the Tx and Rx coils are identical, whereas asymmetrical structure means that the Rx coil is smaller than the Tx coil in this paper. The proposed IPT coils, considering the design parameters in Table 1, are shown in Fig. 7. The core area of the asymmetrical Rx coil is calculated as 66.5 cm^2 and that of the Tx coil is calculated as 100 cm^2, which means the size of the asymmetrical Rx coil is approximately two-thirds of the Tx coil size. These obvious differences for coil size and coil distance are enough to verify the universality of the proposed design methodology. Note that the thickness of the core t_{c1} and t_{c2} are arbitrarily determined as the first variable parameter of this design procedure: t_{c1} and t_{c2} are selected as 3 mm, and these values will be verified by a simulation analysis to determine the magnetic field density level generated inside the ferrite core. In Fig. 7(a), the distance between the Tx and Rx coils d_c is 40 mm and 20 mm for the symmetry and asymmetry cases, respectively, considering the different size of the Rx coil. The winding turns for N_1 and N_2 are wound from outer to inner directions, and the starting point of the winding turns is the 5% gap of the core width from the outer side, as shown in Fig. 7(b).

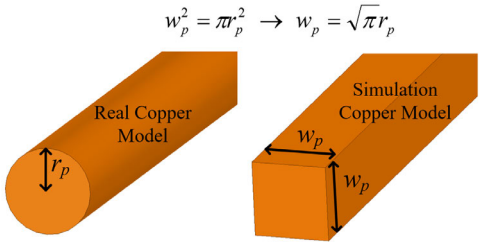

(a) The simulation model of copper for the same current path area.

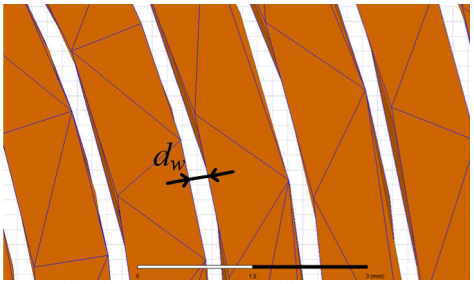

(b) The shape of copper with a FEM mesh.

FIGURE 8. Simulation model of the Tx and Rx coils.

To derive the power efficiency w.r.t. only N_1 and N_2, which are the final target parameters of this paper, the values of r_1, r_2, L_1, and L_2 are defined as functions of N_1 and N_2, as follows:

$$r_1(N_1) = r_{1o}N_1^{\beta_{r1}}, \quad r_2(N_2) = r_{2o}N_2^{\beta_{r2}} \tag{8a}$$

$$L_1(N_1) = L_{1o}N_1^{\beta_{L1}}, \quad L_2(N_2) = L_{2o}N_2^{\beta_{L2}}, \tag{8b}$$

where r_{1o}, r_{2o}, L_{1o}, and L_{2o} are the resistance and inductance coefficients, and β_{r1}, β_{r2}, β_{L1}, β_{L2} are exponential terms of these resistance and inductance values. The parameters of (8) are generally determined by the physical dimension of the Tx and Rx coils and the distance between the Tx and Rx coils d_c with the size of the copper and the characteristics of the ferrite core.

From (8), the magnetizing inductance L_m in (7) can be derived by magnetic coupling coefficient, as follows:

$$k = \frac{nL_m}{\sqrt{L_1 L_2}} \rightarrow \therefore L_m = k\sqrt{L_{1o}L_{2o}}N_1^{0.5\beta_{L1}+1}N_2^{0.5\beta_{L2}-1} \tag{9}$$

where the slight variation of k when the number of turns changes will be reflected to the simulation process in this paper.

Based on equations (7)-(9), the simulation analysis of Fig. 7 is conducted using a FEM based Maxwell 3D simulation tool. The simulation model for copper of the Tx and Rx coils is described in Fig. 8. Even though the copper model is based on a circle-shape, a square simulation model of the copper coil is selected for fast adaptive mesh refinement of the FEM simulation analysis [34]. Note that if the copper area is the same for the real and simulation models, then the copper loss is also the same for both cases, as described in Fig. 8(a) [35]. Because the load current I_L is 4.0 A in Table 1, I_2 is approximately calculated as 4.4A from (2a). Considering the fact that AWG 17 wire (=1.04 mm^2) has 8.0A ampacity, according to NFPA 70, w_p in Fig. 8(a) is

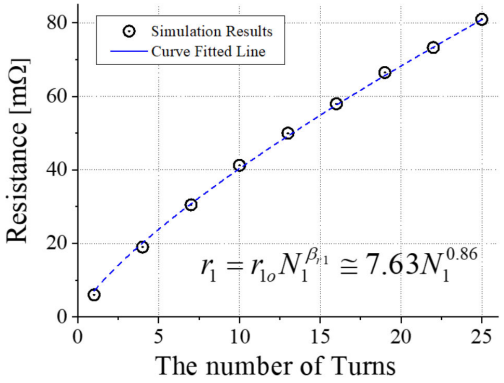

(a) The primary and secondary resistance.

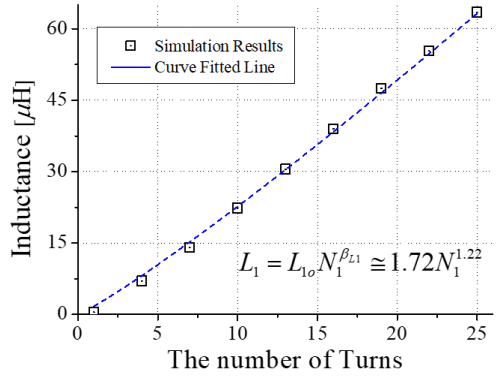

(b) The primary and secondary inductance.

FIGURE 9. Curve fitting results of the resistance and inductance for the symmetry case.

selected as 1 mm for the simulation coil model, which is enough to carry 4.4A coil current [36], [37]. Thus, r_p in Fig. 8(a) is calculated as 0.563mm for the real coil model, which will be used for experimental verification. Because high-frequency litz wire will be used for the experimental verification, a stranded wire model has been selected in the simulation. The distance between copper wires d_w in Fig. 8(b) is selected as 0.3 mm, considering the insulation level between copper wires. The plane-shaped Mn-Zn ferrite core PM11 made by TODAISU was chosen for the Tx and Rx cores [43]. The magnetic loss tangent, i.e., the ratio of real and imaginary permeability, which represents the core loss term, has been reflected to the FEM simulation conditions, according to the datasheet [43], [44]. From the 3D FEM simulation results, equivalent coil loss resistance, including the copper loss and core loss, r_1 and r_2 can be found. The simulation results of (8) are shown in Fig. 9, which is one of the examples for the symmetrical case. From the simulation results by the FEM simulation, the numerical results of non-linear curve fitting can be obtained, as shown in Fig. 9. The remaining simulation results are listed in Table 2, whose values will be used for the proposed IPT design procedure.

III. DESIGN PROCEDURE OF THE PROPOSED IPT

From the given parameters of Table 1 and the obtained parameters of Table 2, the major design parameters of N_1 and N_2 and

TABLE 2. Simulation results of the symmetry and asymmetry parameters.

Parameters	Symmetry case Values	Asymmetry case Values
r_{1o} [mΩ]	7.63	5.94
r_{2o} [mΩ]	7.63	5.10
L_{1o} [μH]	1.72	1.12
L_{2o} [μH]	1.72	1.14
β_{r1}	0.86	0.94
β_{r2}	0.86	0.84
β_{L1}	1.22	1.42
β_{L2}	1.22	1.19

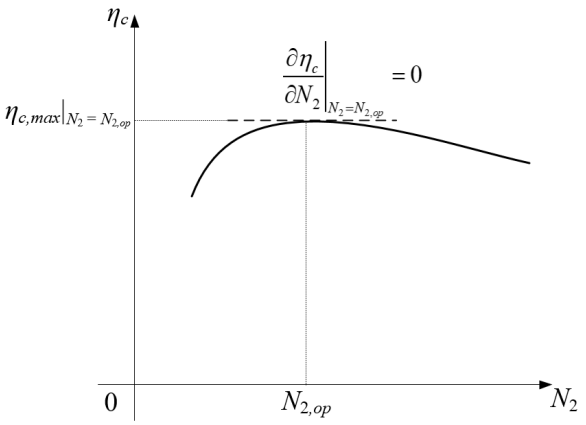

FIGURE 10. Design characteristic of the efficiency w.r.t. N_2 when arbitrary N_1 is chosen.

the design results of the parameters, e.g., η_c, V_{dc}, C_1, C_2, t_{c1}, and t_{c2}, should be determined to complete the proposed IPT procedure. It is noteworthy that only coil-to-coil efficiency is considered and the DC-to-DC efficiency will not be evaluated in order to focus on the determination of the number of turns throughout this paper.

Based on the calculation and simulation results of (7)-(9), as the first step in this design procedure, the maximum power efficiency point when $N_2 = N_{2,op}$ can be found, as shown in Fig. 10, where N_1 is arbitrarily chosen in this step. For the second step, by the same principle as in Fig. 10, various N_1 cases, satisfying $N_2 = N_{2.op}$, should be investigated, as shown in Fig. 11, where N_2 is already chosen as the optimum value for the maximum power efficiency. By comparing various N_1 cases, the optimum values of N_1 and N_2 with the maximum power efficiency can be found. The process to find $N_{2,\mathrm{op}}$ and $N_{1,\mathrm{op}}$ described in Figs. 10-11 is one of design examples proposed in this paper for simplicity of design procedure. From those intuitive and repetitive process of Figs. 10-11, all the N_1 and N_2 combinations have been investigated to find optimal $\mathrm{N_1}$ and $\mathrm{N_2}$ by the proposed 3D FEM analysis. Note that input voltage V_1 in (2a) is determined by the DC voltage V_{dc} and is related

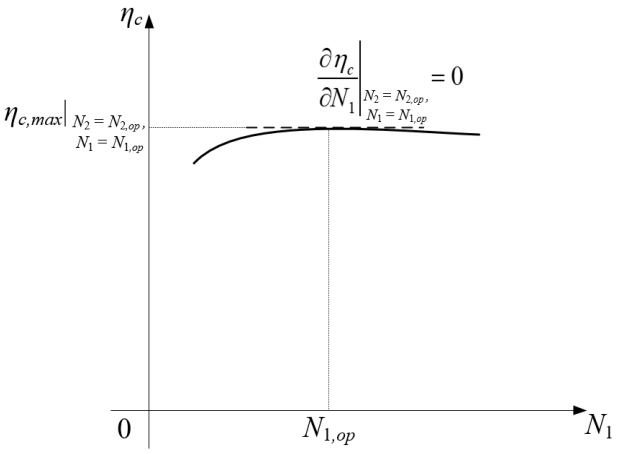

FIGURE 11. Design characteristic of the efficiency w.r.t. N_1 when $N_2 = N_{2,op}$.

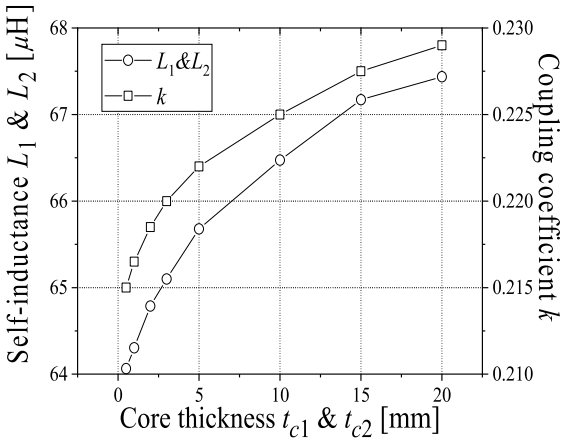

FIGURE 12. Simulation results of the self-inductance and coupling coefficient w.r.t. t_{c1} and t_{c2}, when $N_1 = N_2 = 25$ turns and $d_c = 40$ mm.

to the load power in (4); hence, the target load power P_L can be determined by modulating V_{dc}. It is noteworthy that the value of V_{dc} can be provided and modulated by the AC/DC power supply adopter, which can be freely selected in markets. The resonant capacitors C_1 and C_2 are selected by (3c) for full resonant conditions. Because the magnetic flux density of the ferrite core cannot be confirmed by experiment, such magnetic flux density inside the ferrite core should be identified by a simulation analysis. It is noteworthy that the thickness of the ferrite core t_{c1} and t_{c2} is not largely affected to the major parameters in this paper, e.g., inductance, resistance, and coupling coefficient, whose values have already been derived and evaluated to determine $N_{1,op}$ and $N_{2,op}$. Simulation results of such influence w.r.t. t_{c1} and t_{c2} are shown in Fig. 12, where the self-inductance and coupling coefficient variations were below 5% and 6% when t_{c1} and t_{c2} are largely changed from 0.5 mm to 20 mm. Such slight variations are sufficiently negligible that they do not affect previous steps of the proposed design procedure. Throughout this IPT design procedure, all the electrical and physical

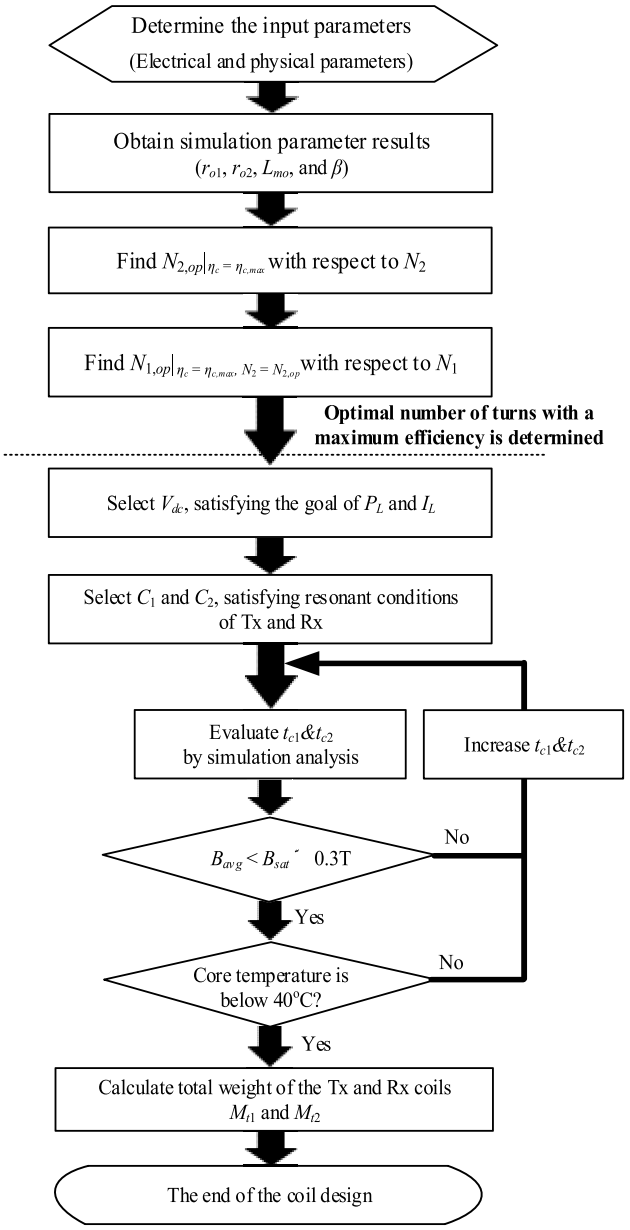

FIGURE 13. Design procedure of the proposed IPT.

parameters can be determined and the total weight of the Tx and Rx coils M_{t1} and M_{t2} can be finally calculated. The IPT design procedure is summarized in Fig. 13 and the validity of the proposed IPT design procedure will be verified experimentally.

IV. EXPERIMENTAL VERIFICATION

A. FABRICATIONS OF THE IPT SYSTEMS

The proposed IPT design procedure discussed in the previous sections has been evaluated by an experimental setup, as shown in Fig. 14. To provide the appropriate DC voltage V_{dc} for the load power P_L, a DC power supply in the source side and a DC electronic load in the load side were used. High-frequency low equivalent-series-resistance (ESR)

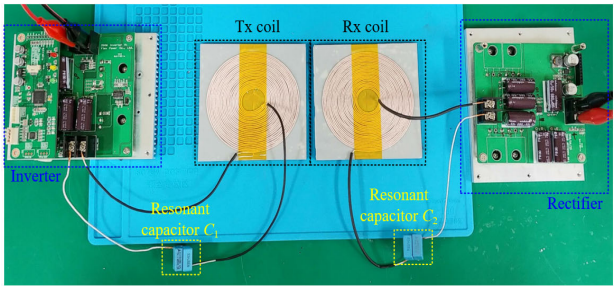

FIGURE 14. An experimental setup for experimental verification in case of symmetry coil structure case.

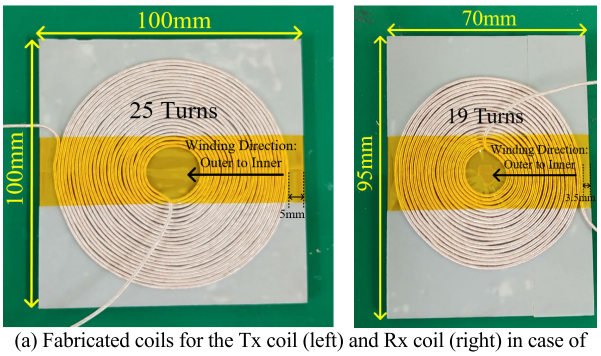

(a) Fabricated coils for the Tx coil (left) and Rx coil (right) in case of an asymmetry case.

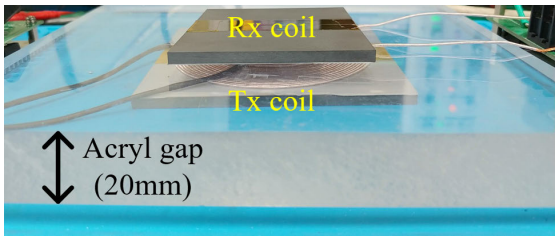

(b) The Tx and Rx coils with 20mm acryl gap for an asymmetry case.

FIGURE 15. Fabricated Tx and Rx coils with acryl gap.

film resonant capacitors were used and the capacitance values are modulated for (3c) by precisely changing the resonant capacitors. To operate a switching frequency of 100 kHz, 0.1mm/60EA type litz wire was adopted for Tx and Rx coils. The thickness of the litz wire was measured as 1.31 mm, which corresponds to the simulation model of Fig. 8, considering the insulation thickness of the wire. The thickness of the ferrite core was selected as 3 mm, which is commercially available in markets, as one of the examples. In Tx system, MCU controller dsPIC33EP32MC202 is used to generate the gate signals. The operating semiconductor switch for high-frequency inverter in the Tx system is selected as 100V IRF540, and 35V schottky diode MBRF2035 is used for the rectifier in the Rx system. To verify the characteristics of the IPT coils w.r.t. the winding turns, the Tx and Rx coils were fabricated, as shown in Fig. 15(a). Note that the maximum number of the turns for N_1 and N_2 in Fig. 15(a) is 25 and 19 turns, respectively, throughout this paper. To apply the distance d_c between the Tx and Rx coils, an acryl panel was used, as shown in Fig. 15(b). It is noted that the material applied in Tx and Rx systems for cases in Fig. 1 is plastic, which is the same characteristics as acryl, i.e., non-conductive and non-magnetic characteristics like insulator. To find the optimal number of turns, satisfying the maximum power transfer efficiency, under the specified condition, i.e., Table 1 in this paper, other electrical and physical parameters are assumed to be fixed; hence, misalignment issues are not considered in this paper. In this experimental verification, the input and output powers P_1 and P_2 in Fig. 2 were measured by AC digital power meters and an oscilloscope. To confirm the AC powers of P_1 and P_2, DC powers of P_s and P_L in Fig. 2 were also measured and the conduction and switching losses are subtracted from P_s and P_L. These values are compared to the results of P_1 and P_2 measured by an oscilloscope and proven to be valid for the experimental verification. To guarantee zero-voltage switching (ZVS) operation of the inverter in Fig. 14, the resonant frequency of the primary side in (3c) determined by C_1 and L_1 was selected as 98 $\sim$ 100 kHz. Although this resonant frequency is slightly lower than a switching frequency, such slight difference has not effect on the coil-to-coil efficiency [38]. All the parameter conditions for experimental verifications are the same as the simulation conditions of Table 1. Passive component tolerance will not be considered in this paper in order to focus on the validity of the proposed design methodology.

To verify the curve fitted simulation results of Fig. 9, the resistance and inductance of the Tx and Rx coils for both symmetrical and asymmetrical cases were measured and compared with the simulation results of Table 2, as shown in Fig. 16. Note that measured resistance r_c in Fig. 16(a)-(b) includes the copper and core loss resistance. The error rates between the simulation and measured results for exponential terms, i.e., β_{r1}, β_{r2}, β_{L1}, β_{L2} are calculated as 4.4 $\sim$ 7.0%; this discrepancy may come from the LCR meter measurement and simulation conditions. To separate the core and copper resistance from Fig. 16, the core resistance r_{co} and copper resistance r_{cp} for two coil cases were simulated and measured, as shown in Fig. 17. The copper resistance r_{cp} was measured without the ferrite core condition, and the core resistance r_{co} is calculated by r_c minus r_{cp} ($r_{co} = r_c$ - r_{cp}). In this experimental prototype for two coil cases, the core resistance and copper resistance are approximately 90% and 10% of the coil loss, respectively. Note that this ratio of core and copper resistance could be changed for different physical and electrical conditions. Through Figs. 16-17, it has been identified that the simulation model of Figs. 7-8 is valid for the proposed IPT design procedure.

B. SYMMETRICAL Tx AND Rx COIL STRUCTURE CASE

To verify the proposed IPT design procedure, a symmetrical coil structure for the Tx and Rx coils was fabricated, as shown in Fig. 14, where $l_{c1} = l_{c2} = w_{c1} = w_{c2} = 100$ mm in this case. As the first step to determine N_1 and N_2, the optimum number of secondary turns $N_{2,op}$ should be found, as described in Fig. 10. To implement the experiments for

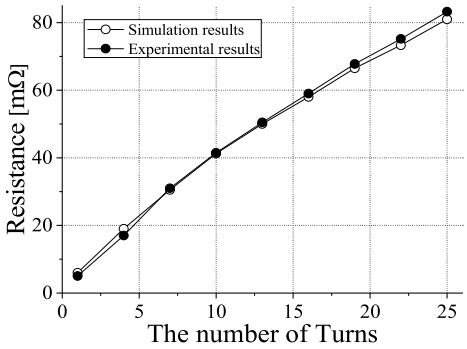

(a) Resistance w.r.t. turns for l_{c1} = 100mm and w_{c1} = 100mm coil case.

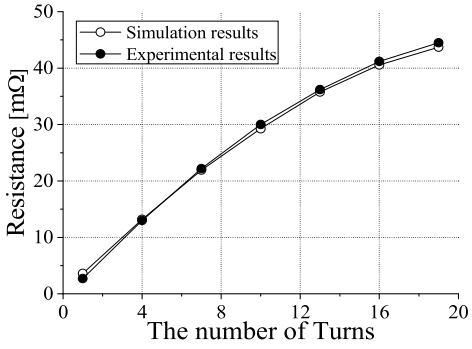

(b) Resistance w.r.t. turns for l_{c1} = 95mm and w_{c1} = 70mm coil case.

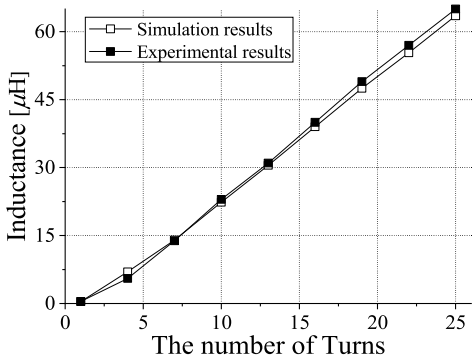

(c) Inductance w.r.t. turns for l_{c1} = 100mm and w_{c1} = 100mm coil case.

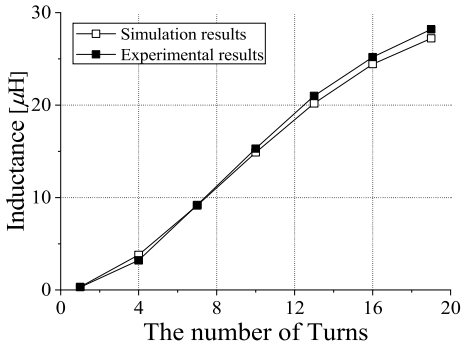

(d) Inductance w.r.t. turns for l_{c1} = 95mm and w_{c1} = 70mm coil case.

FIGURE 16. Comparison of measured and curve fitted simulation results for resistance and inductance in case of two coils.

finding the maximum power efficiency in Fig. 13, the load resistance is set as 2.5 Ω, and 40W load power can be satisfied by modulating V_{dc}. When the number of turns is changed,

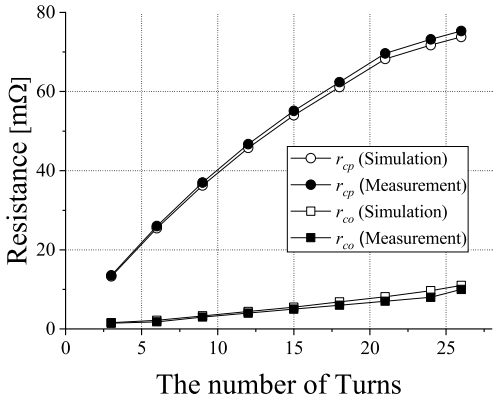

(a) l_{c1} = 100mm and w_{c1} = 100mm coil case.

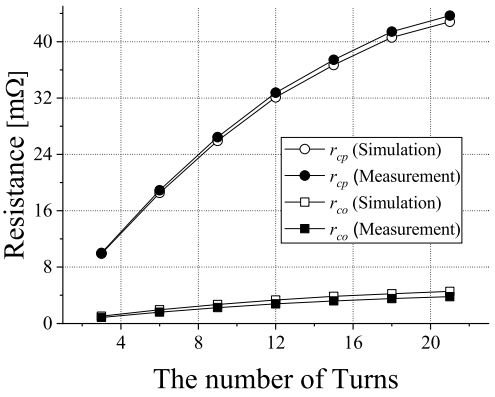

(b) l_{c1} = 95mm and w_{c1} = 70mm coil case.

FIGURE 17. Measured and simulated core and copper resistance for two coil cases.

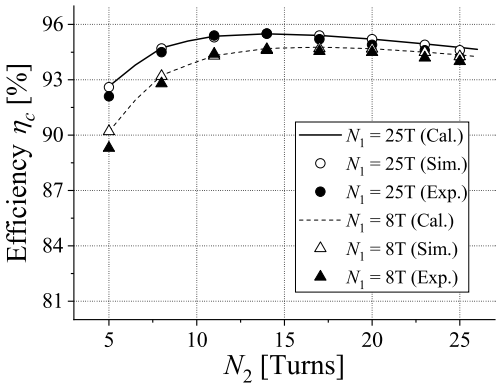

FIGURE 18. Comparison of the coil-to-coil efficiency w.r.t. N_2 for the symmetry case.

the resonant capacitors were precisely turned for resonant conditions of (3c). The experimental results as well as the simulation and calculation results are shown in Fig. 18, where the simulation results were performed by a PSIM simulation tool and only two cases for $N_1 = 25$ and 8 turns were introduced as an example. From the results of Fig. 18, $N_{2,op}$ can be found as 14 and 19 turns for $N_1 = 25$ and 8 turns, respectively. The characteristics of the power efficiency w.r.t. N_1 under $N_2 = N_{2,op}$ is shown in Fig. 19. $N_{2,op}$ decreases when N_1 increases for the maximum power efficiency point,

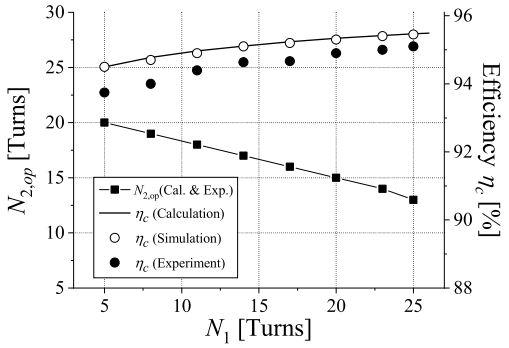

FIGURE 19. The results of the coil-to-coil efficiency and $N_{2,op}$ w.r.t. N_1 for the symmetry case.

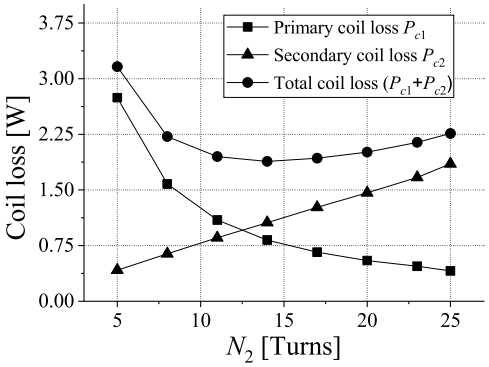

FIGURE 20. The results of the coil loss w.r.t. N_2 when $N_1 = N_{1,op} = 25$ turns for the symmetry case.

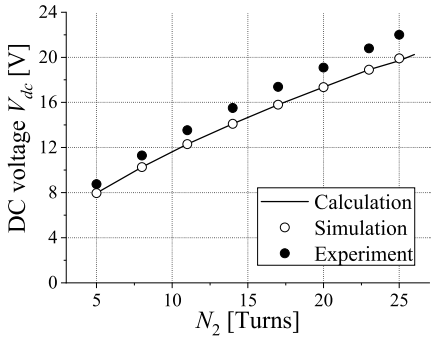

FIGURE 21. Comparison of DC voltage V_{dc} w.r.t. N_2 when $N_1 = N_{1,op} = 25$ turns, satisfying $P_L = 40$W, for the symmetry case.

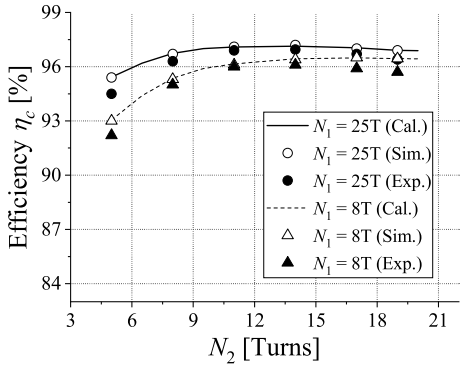

FIGURE 22. Comparison of the coil-to-coil efficiency w.r.t. N_2 for the asymmetrical case.

as shown in Fig. 19, and the tendency of the characteristics w.r.t. N_1 and N_2 in Figs. 18-19 is the same for the calculation and experiment results. A major discrepancy between the calculation and experiment in Figs. 18-19 comes from an additional loss by an ESR of the resonant capacitors, which is not considered in the calculation results.

To confirm the loss characteristics of the proposed IPT, the primary and secondary coil losses including core and copper losses P_{c1} and P_{c2} are shown in Fig. 20, where only one case for $N_1 = 25$ turns is introduced as an example. From the results of Fig. 20, a minimum loss point exists, i.e., $N_2 = 14$ turns, which is in good agreement with the maximum power transfer efficiency point in Fig. 18; hence, $N_{1,op} = 25$ and $N_{2,op} = 14$ for the symmetrical case. The measured maximum power efficiency operating at the maximum power efficiency is 95.1% and the error rate between the calculated and measured results is 0.31%.

To satisfy the load power requirement in Fig. 13, V_{dc} should be modulated for $P_L = 40$W, as shown in Fig. 21, where only one case for $N_1 = 25$ turns is introduced as an example. V_{dc} increases when N_2 increases for $P_L = 40$W and V_{dc} can be found as 15.5V for $N_1 = N_{1,op}$ and $N_2 = N_{2,op}$; hence, the AC/DC power supply, providing 15.5V, can be used in this case. The discrepancy between the calculation and experiment results comes from the slight difference of the primary resonant frequency for the ZVS operation of the inverter.

C. ASYMMETRICAL Tx AND Rx COIL STRUCTURE CASE

To verify the universality of the proposed IPT design procedure and compare with the characteristics of the symmetrical case, an asymmetrical Tx and Rx coil structure is built and evaluated: $l_{c1} = 100$ mm, $w_{c1} = 100$ mm for the Tx coil and $l_{c2} = 95$ mm, $w_{c2} = 70$ mm for the Rx coil, as shown in Fig. 15. As identified from the previous experimental results, all the experimental results of the asymmetrical coil case were compared with the calculation and simulation, as shown in Figs. 22-23. From the results of Fig. 22, $N_{2,op}$ can be found as 13 and 19 turns for $N_1 = 25$ and 8 turns, respectively, whose results are similar with a symmetry case. From Fig. 23, the measured maximum power efficiency operating at a maximum power efficiency is 96.8%. This value is slightly larger than the symmetrical case, due to the relatively large magnetic coupling coefficient compared to the symmetrical case, although the Rx coil of the asymmetrical case is smaller than that of the symmetrical case. In this case, the error rate between the calculated and measured value is 0.27%. From these results of Figs. 22-23, an optimum design point of N_1 and N_2 is found to be $N_{1,op} = 25$ and $N_{2,op} = 13$ for the asymmetrical case. The tendencies of the coil loss and V_{dc} w.r.t. N_2 are similar with the symmetrical coil case, as shown

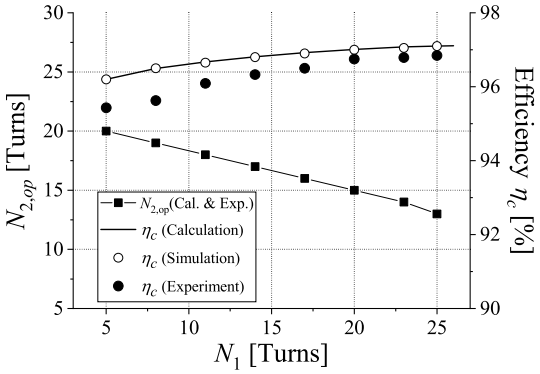

FIGURE 23. The results of the coil-to-coil efficiency and $N_{2,op}$ w.r.t. N_1 for the asymmetrical case.

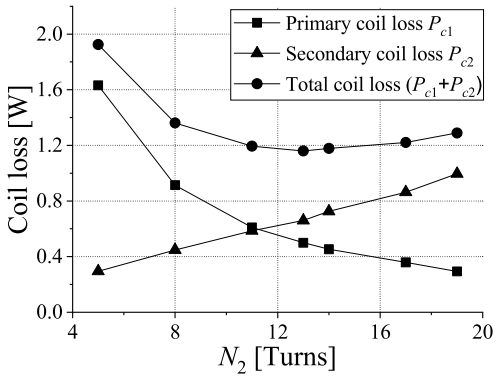

FIGURE 24. The results of the coil loss w.r.t. N_2 when $N_1 = 25$ turns for the asymmetrical case.

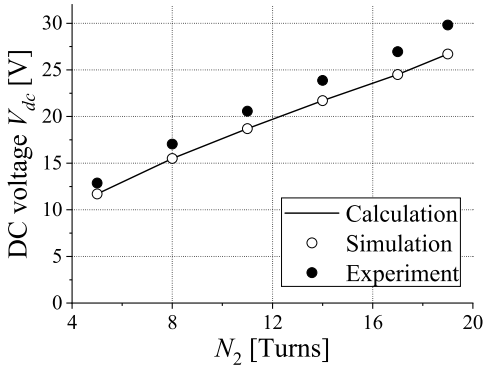

FIGURE 25. Comparison of DC voltage V_{dc} w.r.t. N_2 when $N_1 = 25$ turns, satisfying $P_L = 40$W, for the asymmetrical case.

in Figs. 24-25. V_{dc} for $P_L = 40$ W is found to be 21.7V, as shown in Fig. 25, whose value is larger than that of the symmetrical case.

D. SUMMARY OF LOSS ANALYSIS AND EFFICIENCY IMPROVEMENT

To identify the magnetic characteristics of the ferrite core for Tx and Rx coils, a 3D FEM simulation analysis was performed, as shown in Fig. 26, where the optimal operating point for symmetrical case having $N_1 = N_{1,op} = 25$ and

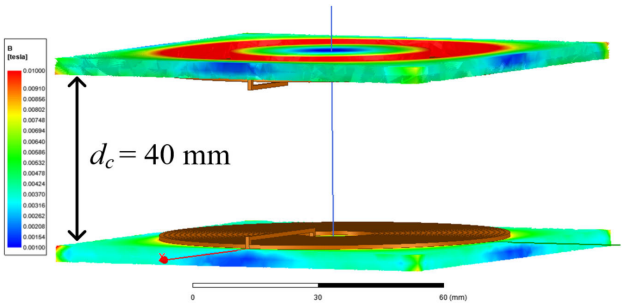

FIGURE 26. Magnetic field distribution inside the Tx and Rx cores for the symmetrical case.

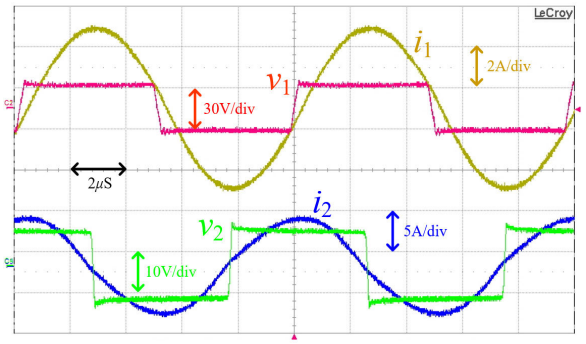

FIGURE 27. An example of experimental waveform for symmetrical case, operating at a maximum power efficiency point.

$N_2 = N_{2,op} = 14$ is selected as one of the representative examples. Due to operating currents of $I_1 = 3.3$A and $I_2 = 4.4$A as an optimum operating point for the maximum power transfer point, ampere-turns for Tx and Rx coils can be calculated as $N_1I_1 = 82.5$ AT and $N_2I_2 = 61.6$ AT. It is noteworthy that the phase difference between I_1 and I_2 is almost 90° if the resonant condition of (3c) is satisfied, as shown in Fig. 27. From the results of the FEM simulation analysis, the average values of B_1 and B_2 for the symmetrical case $B_{1,avg}$ and $B_{2,avg}$ are 20.5 mT and 17.2 mT, respectively, under $N_1I_1 = 82.5$ AT and $N_2I_2 = 61.6$ AT. By the same principle, $B_{1,avg}$ and $B_{2,avg}$ for the asymmetrical case can be found as 17.7 mT and 18.6 mT, respectively, under $N_1I_1 = 65.0$ AT and $N_2I_2 = 57.2$ AT. The remaining measured results are summarized in Table 3.

In order to evaluate the core loss, the Steinmetz equation, given as follows, is widely used [45], [46]

$$P_{cv} = C_m f_s^x B^y \ [kW/cm^3], \tag{10}$$

where C_m, x, and y are the coefficients, which are generally provided by the characteristics of the ferrite core [43].

The quantitative core loss can be assessed for the IPT coils when the amount of core in the Tx and Rx coils is provided. Then, the core loss in the case of the Tx and Rx coils can then be analytically calculated from (10) as follows:

$$P_{co1} = \iiint P_{cv}\, dxdydz = C_m f_s^x B_{1,avg}^y U_1 \ [W], \tag{11a}$$

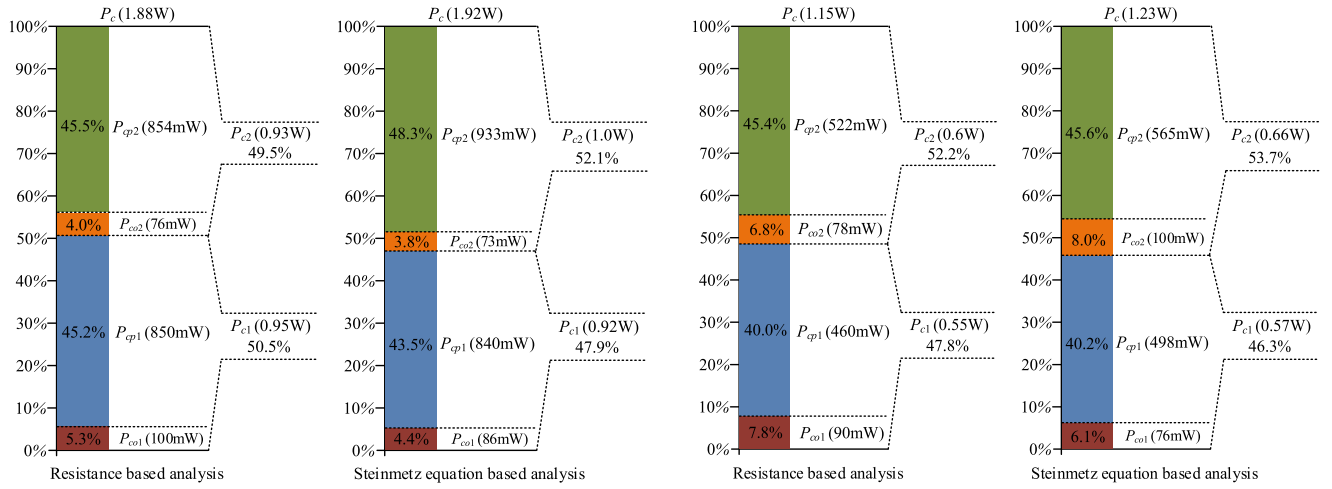

FIGURE 28. Loss analysis of core and copper losses for resistance-based analysis and Steinmetz equation-based analysis.

TABLE 3. Summary of measured characteristics for two cases at an optimal operating point.

Symmetrical coil structure case				Asymmetrical coil structure case			
Parameter	Value	Parameter	Value	Parameter	Value	Parameter	Value
L_1	65.1 μH	r_{co2}	3.9 $m\Omega$	L_1	63.5 μH	r_{co2}	4.0 $m\Omega$
L_2	32.5 μH	r_{cp2}	44.1 $m\Omega$	L_2	21.1 μH	r_{cp2}	27.0 $m\Omega$
k	0.202	I_1	3.3 A	k	0.385	I_1	2.6 A
r_{c1}	87.2 $m\Omega$	I_2	4.4 A	r_{c1}	81.4 $m\Omega$	I_2	4.4 A
r_{co1}	9.2 $m\Omega$	$\eta_{c,max}$	95.1%	r_{co1}	13.3 $m\Omega$	$\eta_{c,max}$	96.8%
r_{cp1}	78.0 $m\Omega$	$B_{1,avg}$	20.5 mT	r_{cp1}	68.0 $m\Omega$	$B_{1,avg}$	17.7 mT
r_{c2}	48.0 $m\Omega$	$B_{2,avg}$	17.2 mT	r_{c2}	31.0 $m\Omega$	$B_{2,avg}$	18.6 mT

$$P_{co2} = \iiint P_{cv}\, dxdydz = C_m f_s^x B_{2,avg}^y U_2 \ [W], \qquad (11b)$$

where U_1 and U_2 are the volume of the ferrite core for the Tx and Rx coils, respectively.

From the datasheet of the ferrite core, the values of C_m, x, and y highly depends on the temperature. For example, $C_m = 44.3$, $x = 1.13$, and $y = 2.20$ at 25°C core temperature and $C_m = 11.1$, $x = 1.31$, and $y = 2.96$ at 100°C core temperature; these values can be obtained by the curved fitted method based on the power loss graph in the datasheet [43]. It has been identified from these results that the value of y decreases when the core temperature decreases. It is noteworthy that the core loss in (11) is proportional to I^y due to $I^y \propto B^y$; hence, the increment level of the core loss depends on the core temperature.

On the other hand, in Fig. 17, the core resistance r_{co} has been obtained by a LCR meter device and the value of r_{co} is fixed when the number of turns is decided. Based on Fig. 17, the core loss can be calculated by $I^2 r_{co}$, which is quite different from the Steinmetz equation-based core loss calculation. Therefore, in order to identify the characteristics of the coil loss, a comparative loss analysis for the Steinmetz equation-based method and the resistance model-based method has been implemented, as shown in Fig. 28, where the IPT system is assumed to be operated at an optimal operating point for the maximum power transfer efficiency. It is assumed that the core temperature is 25°C and the copper loss in the Steinmetz equation-based analysis can be found by the FEM simulation analysis. As shown in Fig. 28, the core loss of P_{co1} and P_{co2} is approximately 10% of the whole coil loss, which corresponds to Fig. 17. The resistance model-based analysis, which is adopted for the proposed design methodology, is good agreement with the Steinmetz equation-based analysis. The measured Tx and Rx core temperatures are below 40°C at a 23°C ambient temperature environment. If core thickness is selected to be less than 3 mm, average value of magnetic field would be closed to the saturated magnetic field, which eventually causes the increment of core temperature and thermal unstable condition; hence, stable operation of the IPT system is guaranteed by 3 mm core thickness, as described in the design procedure of Fig. 13.

As the final step, the total weight of the Tx and Rx coils can be calculated by the volume and density of the ferrite cores and the copper. Considering the densities of the ferrite core and the copper, i.e., 4,850 kg/m^3 and 8.96 g/cm^3, M_{t1} and

TABLE 4. Comparison of efficiency improvement by the proposed design methodology.

Symmetrical coil structure case		Asymmetrical coil structure case	
Comparison advantage	Efficiency improvement	Comparison advantage	Efficiency improvement
N_2 = 5T vs N_2 = 14T (N_1 = 25T)	3.8%	N_2 = 5T vs N_2 = 11T (N_1 = 25T)	2.7%
N_1 = 5T vs N_1 = 25T ($N_2 = N_{2,op}$)	1.4%	N_1 = 5T vs N_1 = 25T ($N_2 = N_{2,op}$)	1.4%

M_{t2} for the symmetrical case are calculated as 232.7 g and 220.9 g, respectively. By same principle, the total weight of M_{t2} for the asymmetrical case is calculated as 140.8 g.

The efficiency improvement by the proposed design methodology is summarized in Table 4. In the case of a symmetrical example, the efficiency improvement is 3.8% by only changing N_2 when $N_1 = 25$ turns in Fig. 18 and 1.4% by only changing N_1 when $N_2 = N_{2,op}$ in Fig. 19. In the case of an asymmetrical example, the efficiency improvement is 2.7% by only changing N_2 when $N_1 = 25$ turns in Fig. 22 and 1.4% by only changing N_1 when $N_2 = N_{2,op}$ in Fig. 23. The efficiency improvement obtained by the proposed design methodology is expected to be beneficial to reduce the coil heating problem.

V. CONCLUSION

The proposed IPT design methodology to determine the optimal number of turns having the maximum power transfer efficiency is found to be a useful and practical solution for laptop wireless charging applications in this paper. When the load characteristics and physical size of Tx and Rx cores, which are inherently given for the laptop wireless charging applications, are specified for the IPT design, the optimum values of N_1 and N_2 can be determined for operating at the maximum power efficiency. By utilizing a FEM simulation analysis, electrical characteristics of resistance and inductance for the IPT coils, which are theoretically impossible to be analyzed due to the magnetic field distortion by the non-linear property of ferrite core, can be obtained. Contrary to the conventional coil design methodologies [31]–[33], the proposed design methodology can be utilized for an IPT system employing a ferrite core. By selecting optimal number of turns derived from the proposed IPT design methodology, 3.8% and 2.7% of power efficiency have been improved. By virtue of the proposed IPT design method, the trial-and-error process to find the optimum turns of the IPT coils for the maximum power efficiency can be greatly reduced.

REFERENCES

[1] D. Lin, C. Zhang, and S. Y. R. Hui, "Mathematic analysis of omnidirectional wireless power transfer—Part-II three-dimensional systems," *IEEE Trans. Power Electron.*, vol. 32, no. 1, pp. 613–624, Jan. 2017.

[2] C. Zhang, D. Lin, and S. Y. Hui, "Basic control principles of omnidirectional wireless power transfer," *IEEE Trans. Power Electron.*, vol. 31, no. 7, pp. 5215–5227, Jul. 2016.

[3] C. Park, S. Lee, G. Cho, S. Choi, and C. T. Rim, "Two-dimensional inductive power transfer system for mobile robots using evenly displaced multiple pickups," *IEEE Trans. Ind. Appl.*, vol. 50, no. 1, pp. 538–565, Jun. 2013.

[4] B. H. Choi, E. S. Lee, Y. H. Sohn, G. C. Jang, and C. T. Rim, "Six degrees of freedom mobile inductive power transfer by crossed dipole TX and RX coils," *IEEE Trans. Power Electron.*, vol. 31, no. 4, pp. 3252–3272, Apr. 2016.

[5] M. Budhia, J. T. Boys, G. A. Covic, and C.-Y. Huang, "Development of a single-sided flux magnetic coupler for electric vehicle IPT charging systems," *IEEE Trans. Ind. Electron.*, vol. 60, no. 1, pp. 318–328, Jan. 2013.

[6] R. Bosshard, J. W. Kolar, J. Mühlethaler, I. Stevanović, B. Wunsch, and F. Canales, "Modeling and $\eta - \alpha$-Pareto optimization of inductive power transfer coils for electric vehicles," *IEEE J. Emerg. Sel. Topics Power Electron.*, vol. 3, no. 1, pp. 50–64, Mar. 2015.

[7] V. Shevchenko, O. Husev, R. Strzelecki, B. Pakhaliuk, N. Poliakov, and N. Strzelecka, "Compensation topologies in IPT systems: Standards, requirements, classification, analysis, comparison and application," *IEEE Access*, vol. 7, pp. 120559–120580, 2019.

[8] J. Deng, W. Li, T. D. Nguyen, S. Li, and C. C. Mi, "Compact and efficient bipolar coupler for wireless power chargers: Design and analysis," *IEEE Trans. Power Electron.*, vol. 30, no. 11, pp. 6130–6140, Nov. 2015.

[9] S. Li and C. Chris Mi, "Wireless power transfer for electric vehicle applications," *IEEE J. Emerg. Sel. Topics Power Electron.*, vol. 3, no. 1, pp. 4–17, Mar. 2015.

[10] G. R. Nagendra, G. A. Covic, and J. T. Boys, "Determining the physical size of inductive couplers for IPT EV systems," *IEEE J. Emerg. Sel. Topics Power Electron.*, vol. 2, no. 3, pp. 571–583, Sep. 2014.

[11] J. H. Kim, B.-S. Lee, J.-H. Lee, S.-H. Lee, C.-B. Park, S.-M. Jung, S.-G. Lee, K.-P. Yi, and J. Baek, "Development of 1-MW inductive power transfer system for a high-speed train," *IEEE Trans. Ind. Electron.*, vol. 62, no. 10, pp. 6242–6250, Oct. 2015.

[12] S. Lee, B. Choi, and C. T. Rim, "Dynamics characterization of the inductive power transfer system for online electric vehicles by Laplace phasor transform," *IEEE Trans. Power Electron.*, vol. 28, no. 12, pp. 5902–5909, Dec. 2013.

[13] S. Y. Choi, B. W. Gu, S. Y. Jeong, and C. T. Rim, "Advances in wireless power transfer systems for roadway-powered electric vehicles," *IEEE J. Emerg. Sel. Topics Power Electron.*, vol. 3, no. 1, pp. 18–36, Mar. 2015.

[14] J. Huh, S. W. Lee, W. Y. Lee, G. H. Cho, and C. T. Rim, "Narrow-width inductive power transfer system for online electrical vehicles," *IEEE Trans. Power Electron.*, vol. 26, no. 12, pp. 3666–3679, Dec. 2011.

[15] B. H. Choi, E. S. Lee, J. Huh, and C. T. Rim, "Lumped impedance transformers for compact and robust coupled magnetic resonance systems," *IEEE Trans. Power Electron.*, vol. 30, no. 11, pp. 6046–6056, Nov. 2015.

[16] J. Kim, H.-C. Son, K.-H. Kim, and Y.-J. Park, "Efficiency analysis of magnetic resonance wireless power transfer with intermediate resonant coil," *IEEE Antennas Wireless Propag. Lett.*, vol. 10, pp. 389–392, May 2011.

[17] C. K. Lee, W. X. Zhong, and S. Y. R. Hui, "Effects of magnetic coupling of nonadjacent resonators on wireless power domino-resonator systems," *IEEE Trans. Power Electron.*, vol. 27, no. 4, pp. 1905–1916, Apr. 2012.

[18] M. Wang, J. Feng, Y. Shi, and M. Shen, "Demagnetization weakening and magnetic field concentration with ferrite core characterization for efficient wireless power transfer," *IEEE Trans. Ind. Electron.*, vol. 66, no. 3, pp. 1842–1851, Mar. 2019.

[19] B.-Y. Liu, Z.-K. Chen, and H.-M. Hsu, "Efficiency analysis of magnetic resonance wireless power transfer with intermediate resonant coil," in *Proc. IEEE Wireless Power Transf. Conf. (WPTC)*, Jun. 2018, pp. 1–6.

[20] M. Kiani, U.-M. Jow, and M. Ghovanloo, "Design and optimization of a 3-coil inductive link for efficient wireless power transmission," *IEEE Trans. Biomed. Circuits Syst.*, vol. 5, no. 6, pp. 579–591, Dec. 2011.

[21] E. S. Lee, B. G. Choi, J. S. Choi, D. T. Nguyen, and C. T. Rim, "Wide-range adaptive IPT using dipole-coils with a reflector by variable switched capacitance," *IEEE Trans. Power Electron.*, vol. 32, no. 10, pp. 8054–8070, Oct. 2017.

[22] B. H. Choi, V. X. Thai, E. S. Lee, J. H. Kim, and C. T. Rim, "Dipole-coil-based wide-range inductive power transfer systems for wireless sensors," *IEEE Trans. Ind. Electron.*, vol. 63, no. 5, pp. 3158–3167, May 2016.

[23] B. G. Choi, J. H. Kim, E. S. Lee, H. R. Kim, and C. T. Rim, "Optimal dipole-coil ampere-turns design for maximum power efficiency of IPT," *IEEE Trans. Power Electron.*, vol. 35, no. 7, pp. 7317–7327, Jul. 2020.

[24] D. T. Nguyen, E. S. Lee, B. G. Choi, and C. T. Rim, "Optimal shaped dipole-coil design and experimental verification of inductive power transfer system for home applications," in *Proc. IEEE Appl. Power Electron. Conf. Expo. (APEC)*, Mar. 2016, pp. 1773–1779.

[25] V. X. Thai, S. Y. Choi, B. H. Choi, J. H. Kim, and C. T. Rim, "Coreless power supply rails compatible with both stationary and dynamic charging of electric vehicles," in *Proc. IEEE 2nd Int. Future Energy Electron. Conf. (IFEEC)*, Nov. 2015, pp. 1–6.

[26] B. G. Choi, Y.-H. Sohn, E. S. Lee, S. H. Han, H. R. Kim, and C. T. Rim, "Coreless transmitting coils with conductive magnetic shield for wide-range ubiquitous IPT," *IEEE Trans. Power Electron.*, vol. 34, no. 3, pp. 2539–2552, Mar. 2019.

[27] W. Qian, X. Zhang, Y. Fu, J. Lu, and H. Bai, "Applying normally-off GaN HEMTs for coreless high-frequency wireless chargers," *CES Trans. Electr. Mach. Syst.*, vol. 1, no. 4, pp. 418–427, Dec. 2017.

[28] S. Kim, G. A. Covic, and J. T. Boys, "Tripolar pad for inductive power transfer systems for EV charging," *IEEE Trans. Power Electron.*, vol. 32, no. 7, pp. 5045–5057, Jul. 2017.

[29] T. Imura and Y. Hori, "Maximizing air gap and efficiency of magnetic resonant coupling for wireless power transfer using equivalent circuit and Neumann formula," *IEEE Trans. Ind. Electron.*, vol. 58, no. 10, pp. 4746–4752, Oct. 2011.

[30] X. Dai, X. Li, Y. Li, and A. P. Hu, "Impedance-matching range extension method for maximum power transfer tracking in IPT system," *IEEE Trans. Power Electron.*, vol. 33, no. 5, pp. 4419–4428, May 2018.

[31] M. Pinuela, D. C. Yates, S. Lucyszyn, and P. D. Mitcheson, "Maximizing DC-to-Load efficiency for inductive power transfer," *IEEE Trans. Power Electron.*, vol. 28, no. 5, pp. 2437–2447, May 2013.

[32] G. Zhu and R. D. Lorenz, "Achieving low magnetic flux density and low electric field intensity for a loosely coupled inductive wireless power transfer system," *IEEE Trans. Ind. Appl.*, vol. 54, no. 6, pp. 6383–6393, Nov. 2018.

[33] R. Bosshard, J. Muhlethaler, J. W. Kolar, and I. Stevanovic, "Optimized magnetic design for inductive power transfer coils," in *Proc. 28th Annu. IEEE Appl. Power Electron. Conf. Expo. (APEC)*, Long Beach, CA, USA, Mar. 2013, pp. 1812–1819.

[34] M. Wake and R. Yamada, "FEM calculation of magnetization process in a multi-filamentary superconductor," *IEEE Trans. Appl. Supercond.*, vol. 17, no. 2, pp. 3741–3744, Jun. 2007.

[35] H. Shinagaw, T. Suzuki, M. Noda, Y. Shimura, S. Enoki, and T. Mizuno, "Theoretical analysis of AC resistance in coil using magnetoplated wire," *IEEE Trans. Magn.*, vol. 45, no. 9, pp. 3259–3521, Sep. 2009.

[36] *Electric Cables—Calculation of the Current Rating, Part 1: Current Rating Equations (100% Load Factor) and Calculation of Losses, Section 1: General*, Standard IEC 60287-1-1, 2006.

[37] *NFPA 70: National Electrical Code*, 1st ed., Nat. Fire Protection Assoc., Quincy, MA, USA, 2017.

[38] Y. H. Sohn, B. H. Choi, E. S. Lee, G. C. Lim, G. H. Cho, and T. C. Rim, "General unified analyses of two-capacitor inductive power transfer systems," *IEEE Trans. Power Electron.*, vol. 30, no. 1, pp. 6030–6045, Nov. 2015.

[39] C. T. Rim and G. H. Cho, "Phasor transformation and its application to the DC/AC analyses of frequency phase-controlled series resonant converters (SRC)," *IEEE Trans. Power Electron.*, vol. 5, no. 2, pp. 201–211, Apr. 1990.

[40] C. T. Rim, D. Y. Hu, and G. H. Cho, "Transformers as equivalent circuits for switches: General proofs and D-Q transformation-based analyses," *IEEE Trans. Ind. Appl.*, vol. 26, no. 4, pp. 777–785, Jul./Aug. 1990.

[41] C. T. Rim, "Unified general phasor transformation for AC converters," *IEEE Trans. Power Electron.*, vol. 26, no. 9, pp. 2465–2475, Sep. 2011.

[42] E. S. Lee, B. H. Choi, J. P. Cheon, G. C. Lim, B. C. Kim, and C. T. Rim, "Temperature-robust LC3 passive LED drivers with low THD, high efficiency and PF, and long life," *IEEE J. Emerg. Sel. Topics Power Electron.*, vol. 3, no. 3, pp. 829–840, Sep. 2015.

[43] Toda-Isu. *Ferrite Core Datasheet*. [Online]. Available: http://forum.cxem.net/applications/core/interface/file/attachment.php?id=318271

[44] J. Fuzerova, J. Fuzer, P. Kollar, L. Hegedus, R. Bures, and M. Faberova, "Analysis of the complex permeability versus frequency of soft magnetic composites consisting of iron and $Fe_{73}Cu_1Nb_3Si_{16}B_7$," *IEEE Trans. Magn.*, vol. 48, no. 4, pp. 1545–1548, Apr. 2012.

[45] C. P. Steinmetz, "On the law of hysteresis," *Proc. IEEE*, vol. 72, no. 2, pp. 197–221, Feb. 1984.

[46] A. Ayachit and M. K. Kazimierczuk, "Steinmetz equation for gapped magnetic cores," *IEEE Magn. Lett.*, vol. 7, Mar. 2016, Art. no. 1302704.

EUN S. LEE (Member, IEEE) received the B.S. degree in electrical engineering from INHA University, Incheon, South Korea, in 2012, and the M.S. and Ph.D. degrees in nuclear and quantum engineering from the Korea Advanced Institute of Science and Technology, Daejeon, South Korea, in 2014 and 2017, respectively. From 2017 to 2019, he was with the LG Electronics CTO Power Electronics Lab, Seoul, South Korea. Since 2019, he has been a Senior Researcher with the Propulsion System Research Team, Korea Railroad Research Institute, Uiwang, South Korea. His current research interests include power converters, multi-level converters, hydrogen fuel cells, and wireless power transfer systems.

BYEONG G. CHOI (Member, IEEE) received the B.S. degree in mechanical engineering from Pusan National University, Busan, South Korea, in 2015, and the Ph.D. degrees from the School of Electrical Engineering, Korea Advanced Institute of Science and Technology, Daejeon, South Korea, in 2020. Since 2020, he has been a Staff Engineer with the Smart Device Team, Samsung Research, Seoul, South Korea. His current research interests include the field of wireless power transfer systems and machine learning.

MYUNG Y. KIM (Member, IEEE) received the B.S. and M.S. degrees in electrical engineering from ChungAng University, Seoul, South Korea, in 1989 and 1991, respectively. From 1991 to 1995, he was a Senior Researcher with the Traction Research Group of Hyundai Precision and Industries Company, South Korea. Since 1995, he has been with the Korea Railroad Research Institute, Uiwang, South Korea, where he is currently a Principal Researcher. His research interests include wireless power transfer systems and power converter systems especially for railway vehicles.

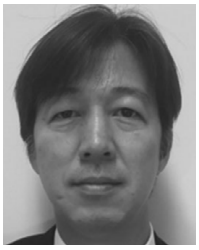

SEUNG H. HAN (Member, IEEE) received the B.S. and M.S. degrees in electrical engineering from the Korea Advanced Institute of Science and Technology (KAIST), Daejeon, South Korea, in 1998 and 2000, respectively. Since 2014, he has been a CEO and CTO of Flex Power Company Ltd. He has been developing various wireless power technologies and products. From 2009 to 2014, he was a CTO of DS Electron Company Ltd., where he has developed various power electronics products including LED drivers for LCD TV and dimming systems for LED lighting.